Fractal dimension estimation for optical image segmentation

H. G. Andrews II & M. A. Getbehead
Rome Laboratory
Photonics Center
Griffiss AFB, NY 13441-4515

S. P. Kozaitis
Florida Institute of Technology
Department of Electrical and Computer Engineering
Melbourne, FL 32901-6988

ABSTRACT

This research investigated the use of fractal dimension measure to segment regions of interest from simulated terrain imagery. The underlying assumption is: a given region of interest in a real-world image has a different fractal dimension than its surrounding terrain. Virtually illuminated, digitally simulated fractal surfaces with known fractal dimensions were investigated. The terrain types that were considered varied from bumpy to flat surfaces. An optically based image segmentation system was constructed to perform the otherwise computationally intensive Fourier transform of the image to be segmented.

1. INTRODUCTION

Previous theoretical and experimental work[1] has established well defined relationships between the topological features of a fractal surface, the illuminated image of that surface, and the power spectrum of the illuminated image. From these relationships, the fractal dimension of an image can be readily estimated by performing an optical Fourier transform and digital post-processing on the power spectrum of the image. From these results, certain inferences can be drawn concerning the location of regions of interest. Namely, features having different fractal dimensions from the surrounding terrain can be spotted quickly using the techniques discussed. This is rationalized by the fact that nature tends to do things in a highly fractal, irregular manner. Manmade objects are generally composed of a series of geometric shapes, straight lines, and smooth curves. These objects will have a different fractal dimension than the terrain upon which they may be located.

This investigation compared the ability of an all digital technique to a hybrid optical-digital technique for estimating the fractal dimension of the computer generated imagery. The digital method performed a fast Fourier transform of the illuminated image, and used that to calculate the image's fractal dimension. The optical-digital technique did essentially the same thing, though the Fourier transform was taken optically. The optical system consisted of a Fourier lens, a 256x256 Semetex Magneto-Optic spatial light modulator (SLM) and a CCD camera at the Fourier plane. Once the Fourier transform was generated, digital post processing calculated the fractal dimension of the original illuminated image. This digital post-processing was identical in both the all digital system and the hybrid optical-digital system.

2. ALGORITHM

Fractal surfaces were generated using the spectral synthesis method[2]. Random two dimensional Fourier components were generated with a mean amplitude of 0 and a standard deviation of

$$\sigma^2 = (i^2 + j^2)^{-(H+1)/2} \tag{1}$$

on the (i,j)th random discrete Fourier component, where H is related to the desired fractal dimension D[3,4] of the surface by

$$D = 2 - H \tag{2}$$

A discrete inverse Fourier transform was then used to generate a fractal surface.

The randomly generated surface was illuminated using a pure Lambertian model where the intensity at a particular location I(x,y) is given by

$$I(x, y) = \cos(p_{x,y}) \tag{3}$$

where $p_{x,y}$ is the angle between the normal of the random surface at (x,y) and the direction to the infinitely distant point source illuminant. The power spectrum, $F_H(f,t)$ of I, is calculated by summing the squares of amplitudes within particular frequency rings. This is then band pass filtered, plotted on a log-log graph, and fitted to a line. There is a linear relationship between the slope -b of the line and the fractal dimension D of the original illuminated image[1,5].

$$D = 3 - \frac{b}{2} \tag{4}$$

3. SURFACE GENERATION AND ILLUMINATION

Twelve surfaces were created using the spectral synthesis method. Illuminating each surface from a variety of angles required knowledge of the normal to the surface at each of the 65,536 points composing the surface. The normal was derived from the partial derivatives (in both x and y) in the usual fashion. Thus, a discrete inverse Fourier transform was used so that the partial derivatives could be numerically approximated. This approach was very compute intensive, and limited the number of Fourier components that could be used.

A total of twelve surfaces were generated. Six used 16x16 Fourier components and the other six used 32x32 components. The H parameter in the spectral synthesis method was varied from 0.0 to 1.0 (inclusive) using an increment of 0.2 in both sets of surfaces. Each of these twelve surfaces was illuminated from six angles, and viewed from directly above. The six angles of illumination varied from 0 to 90 degrees relative to the viewing angle. Each of the 72 images was stored as a 256x256 8-bit gray scale BMP image.

It should be noted at this point that the surfaces are not self shadowing. In order to establish certain baseline characteristics of the algorithm and the optical system's performance, it was decided to remain consistent with the notions established in previous literature on this subject[1]. Additionally, the surfaces considered adhered strictly to the properties of a pure Lambertian illumination model for the same reason.

4. ESTABLISHING BASELINE CHARACTERISTICS

The optical system shown in Figure 1 was used to get optical Fourier transforms of each of the 72 images. The optical setup was capable of taking the Fourier transform only of binarized images. Each gray scale image was thresholded at its average intensity level and placed onto a Semetex model 256i 256x256 magneto-optic SLM. Fourier amplitude information was integrated at the Fourier plane by a CCD camera. This was captured by a frame grabber card, clipped and placed into a binary file for image processing. While the Fourier transform was calculated quite rapidly (the time required for light to propagate from the image on the SLM to the CCD camera), the analog to digital conversion required to capture the image at the Fourier plane took a great deal of time relative to the digital technique described next. This problem can be overcome with better electronic equipment.

The digital technique used the fast Fourier transform (FFT) routines in the Image Pro Plus software package running on a 33MHz 80486DX computer. The FFT of all the illuminated surface images were taken and the amplitude information was stored in BMP binaries; the phase information was discarded. Each Fourier transform required approximately 5 seconds to compute. Figure 2 shows a typical image from its surface contour map, to its illuminated image, to the image of its FFT. An example of the images taken from the optical system was not easily ported into this paper.

The power spectrum of each of the 144 Fourier images was calculated and the data saved to ASCII files. To reduce the effects of noise with the optical system (arising mainly from the pixelation of the SLM), the sections of the optical Fourier transform extending both horizontally and vertically from the DC were blocked out. All of the Fourier transforms were digitally band-pass filtered and the resulting power spectrum was graphed on a log-log plot.

The slope of the line fit to the data in the log-log plots is -b. Equation (4) above was used to calculate D. Tables 1 through 4 show the values for D in each of the 144 Fourier transforms. The H value refers to the parameter for generating the fractal surface, while t refers to the angle of the illumination. With the exception of the extreme cases in illumination angle or the parameter H, the digitally computed values cluster closely to each other for a given fractal dimension. In general, the range of fractal dimension results for a particular value of H do not intrude upon the range calculated for another value of H, though it does occasionally occur.

5. CHARACTERISTICS WHEN DEVIATING FROM THE BASELINE

In Part 4 only the fractal surfaces were considered after illumination from a variety of angles. A geometric shape (such as a square) can be placed over a portion of the illuminated image to see how this changes the fractal dimension measure D from the baseline established in Part 4. (See figure 3.) This was done with both a uniformly shaded square covering the middle of the selected images, and with a square region filled with random 8-bit values (which will be called, for the sake of simplicity here, a uniform pulse and a random pulse respectively). Tables 5 through 8 list the values for D when the digital vs. optical techniques are employed, and when the 16x16 vs. 32x32 Fourier component maps are considered.

In each case, the images were handled identically to those in Part 4 above, and the data was reduced in the same fashion. Due to the large amount of energy in the higher frequencies of the random pulse created by the rapidly changing values within the pulse region, the slope value increase, decreasing the value of b (flattening things out a bit).

The digital approach seems to be reasonably well suited to differentiate between the two pulse types and the un-pulsed data in both the 16x16 and 32x32 Fourier component tests. The difference between the maximum and minimum values is rarely greater than 0.1 save for values of H=1.0 (where all bets are off). The implication is that a deviation greater than 0.1 could indicate a potential region of interest, and may warrant further investigation by either human or electronic processing. Most of the uniform pulse images were at least 0.1 from all of the un-pulsed images with that H value. All of the random pulses were even further away.

Turning attention to the optical setup, we see that there is a bit of a reduction in the ability to discriminate the random pulse and un-pulsed data. However, in most cases there is still little overlap between the two. The uniform pulse, in this case, was discriminated much more easily than in the all digital implementation. The difference in performance characteristics may have been the result of noise in the Semetex. Upon viewing the output from the SLM, there were several lines of light, parts of which should have been turned off. Additionally, the light passing throughout the SLM at the region containing the random pulse did not appear to be distributed properly which may have contributed to the poor performance. (The Semetex seems to have an aversion to complex images.)

6. PERFORMANCE COMPARISON

Each of the two approaches described here has its strengths and weaknesses relative to the other. The primary advantage of the optical system is that the potential speed is far greater than that offered by any of the reasonably priced digital alternatives. Semetex claims a 50fps frame rate on its 256i. Thus, 250 Fourier transforms can be performed optically in

the time it takes to calculate one FFT on the digital platform used here. This assumes that computer hardware controlling the optical system is capable of retrieving imagery at a minimum of 50fps.

There were a number of disadvantages when using the optical system as well. The optical system seemed to be more prone to noise, and the Semetex requires a great deal of fine tuning to get the image displayed properly on the device. This noise is introduced by non-uniform illumination of the SLM, false polarization of entire rows and columns of pixels in the SLM, and from the pixelation of the SLM. Optical aberrations and alignment problems can add additional noise to the system, all of which degrade its discrimination ability. Additionally, the Semetex often requires more than one write to the array in order to eliminate large horizontal bands of light from passing through the device. And finally, attempts to match Semetex's (optimistic rate of) 50fps on the 256i were met with much disappointment.

The advantages of the digital system involve the ability to reduce the noise levels of the process. Based on the results in the tables below, for a given H value, the fractal dimension measure D seemed to be clustered more closely together in the digital system. FFTs have been sufficiently debugged, and computer performance has become increasingly cost effective, that digital FFTs are offering a serious challenge to the speed benefit derived from optical image processing, especially when considering the time and resources required to write information to the SLM and read that data back from the CCD array. Also, the digital system does not require throwing away as much information as does the optical system. 8-Bit gray scale data can be used in the digital system, while the optical system still is capable of only 1-bit grayscale.

The main disadvantage offered by the digital approach relative to the optical system is the speed. The optical system offers the potential to greatly outstrip the digital system by being able to perform Fourier transforms at the speed of light. Writing the image to the SLM and reading it from the camera are severe bottlenecks; bottlenecks which may be overcome with improvements in optical device and analog to digital conversion technology.

7. CONCLUSIONS

Based on the performance of the techniques discussed, it is possible to segment square pulses from fractal backgrounds based on the fractal dimension measure. This implies that there is some merit in considering how this approach deals with more sophisticated shapes occluding portions of more realistic scenery. Additional investigation is warranted in looking at large or high resolution images which can be scanned to detect areas where abrupt changes in the fractal dimension occur.

Though the capability to view even small (ie. 256x256) images in anything approaching a real time fashion is expensive with the off-the-shelf technology, this technology can be applied to other areas in which that capability is not much of a consideration. These techniques could be employed to highlight regions within images taken by various pieces of medical scanning equipment or to automate the process of searching for regions of interest within aerial or space based reconnaissance imagery. If the technology matures sufficiently to allow for real time image processing, these techniques can be used in airborne search and rescue operations, as well as pre-processing for automated target acquisition.

8. ACKNOWLEDGEMENTS

This work was completed at the Photonics Center of Rome Laboratory, Griffiss AFB, NY.

9. TABLES AND FIGURES

H\t	0^m	18^m	36^m	54^m	72^m	90^m
0.0	2.043	2.005	1.944	1.906	1.905	1.940
0.2	2.123	2.094	2.024	1.973	1.964	2.002
0.4	2.198	2 .172	2.102	2.049	2.038	2.070
0.6	2.236	2.231	2.211	2.188	2.183	2.192
0.8	2.011	2.044	2.114	2.140	2.128	2.109
1.0	1.549	1.606	1.739	1.864	1.870	1.793

Table 1 - Digital fractal dimension results *D* for 16x16 Fourier Components with parameter H and illumination angle t

H\t	0	18	36	54^m	72	90^m
0.0	1.799	1.819	1.781	1.745	1.744	1.766
0.2	1.910	1.920	1.876	1.832	1.828	1.860
0.4	2.043	2.074	2.033	1.986	1.974	2.002
0.6	2.244	2.307	2.286	2.246	2.230	2.260
0.8	2.261	2.432	2.510	2.522	2.518	2.509
1.0	1.751	2.072	2.311	2.434	2.442	2.351

Table 2 - Digital fractal dimension results *D* for 32x32 Fourier Components with parameter H and illumination angle t

H\t	0	18^m	36	54^m	72	90^m
0.0	1.707	1.765	1.652	1.613	1.704	1.776
0.2	1.745	1.713	1.732	1.685	1.765	1.824
0.4	1.735	1.740	1.700	1.809	1.828	1.844
0.6	1.853	1.791	1.790	1.760	1.805	1.836
0.8	1.845	1.806	1.876	1.823	1.872	1.900
1.0	1.765	1.989	2.013	1.960	1.996	1.965

Table 3 - Optical results; 16x16 Components on H; illumination angle t

H\t	0	18^m	36^m	54^m	72^m	18^m
0.0	1.517	1.803	1.804	1.715	1.651	1.784
0.2	1.503	1.804	1.803	1.581	1.667	1.868
0.4	1.448	1.658	1.494	1.514	1.709	1.837
0.6	1.473	1.459	1.527	1.602	1.784	1.828
0.8	1.402	1.718	1.611	1.752	1.817	1.847
1.0	1.759	1.885	1.814	1.833	1.823	1.873

Table 4 - Optical results; 32x32 Components on H; illumination angle t

H\.t	18^m	36^m	54^m	72^m
0.4 Random	1.164	1.212	1.248	1.249
0.4 Uniform	2.015	1.994	1.979	1.976
0.6 Random	1.097	1.124	1.150	1.145
0.6 Uniform	1.992	2.018	2.033	2.051

Table 5 - Digital results; 16x16 Components on H; illumination angle t; Random or Uniform Pulse

H\t	18^m	36^m	54^m	72^m
0.4 Random	1.330	1.418	1.462	1.467
0.4 Uniform	1.973	1.969	1.942	1.940
0.6 Random	1.233	1.322	1.370	1.370
0.6 Uniform	2.071	2.106	2.113	2.126

Table 6 - Digital results; 32x32 Components on H; illumination angle t; Random or Uniform Pulse

H\t	18^m	36^m	54^m	72^m
0.4 Random	1.688	1.739	1.616	1.590
0.4 Uniform	2.183	2.016	1.958	1.960
0.6 Random	1.779	1.692	1.681	1.691
0.6 Uniform	2.224	2.062	2.037	1.992

Table 7- Optical results; 16x16 Components on H; illumination angle t; Random or Uniform Pulse

H\t	18^m	36^m	54^m	72^m
0.4 Random	1.790	1.867	1.832	1.810
0.4 Uniform	2.185	2.084	2.066	2.036
0.6 Random	2.005	1.870	1.785	1.735
0.6 Uniform	2.071	2.106	2.113	2.126

Table 8 - Optical results; 32x32 Components on H; illumination angle t; Random or Uniform Pulse

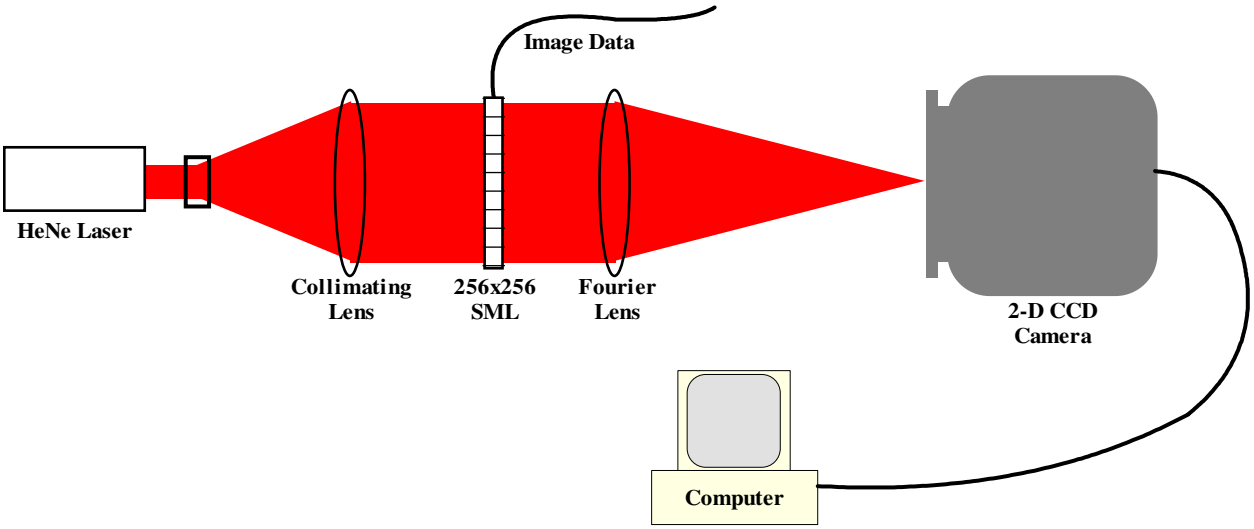

Figure 1 – Optical Setup for Fourier Transform

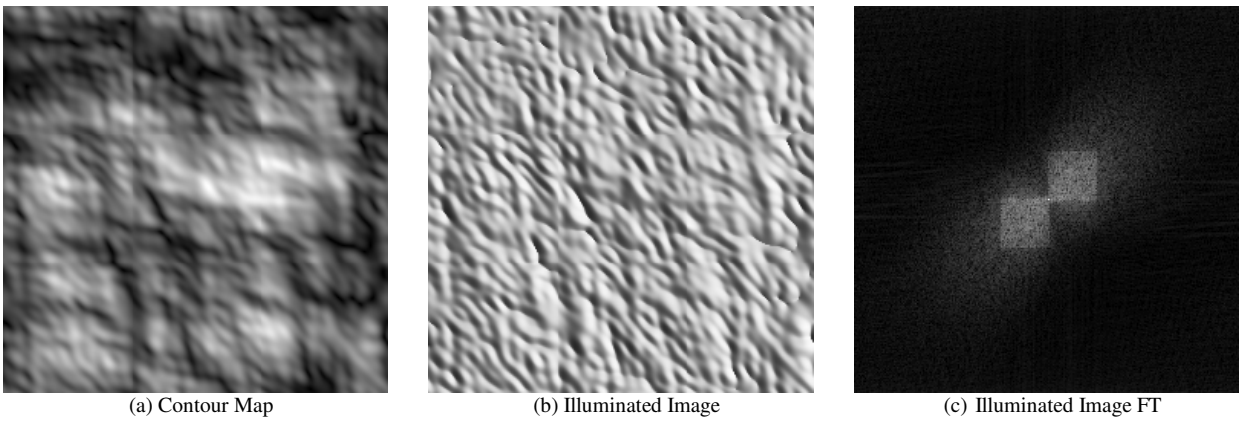

(a) Contour Map (b) Illuminated Image (c) Illuminated Image FT

Figure 2 - Sample Digital Images

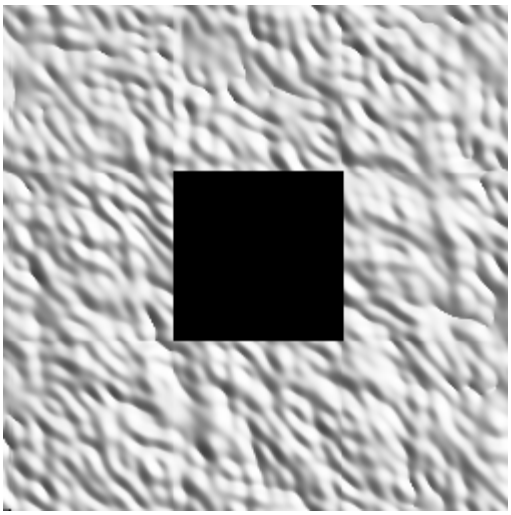

(a) Uniform pulse image

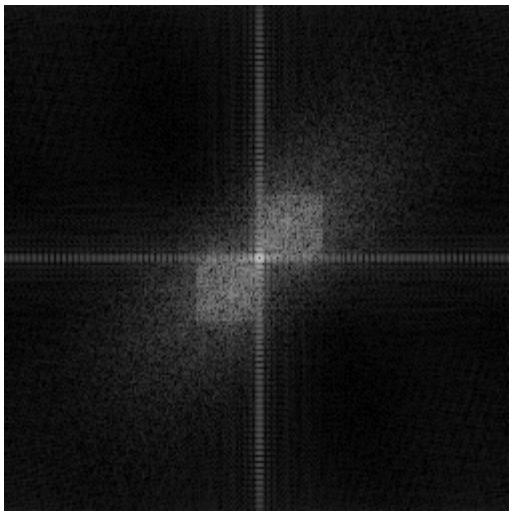

(b) FT of uniform pulse

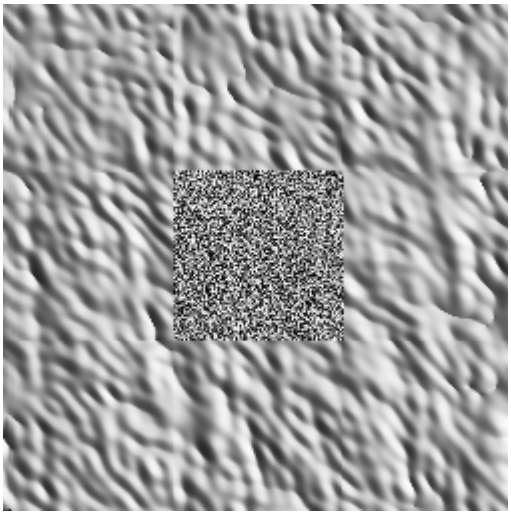

(c) Random pulse image

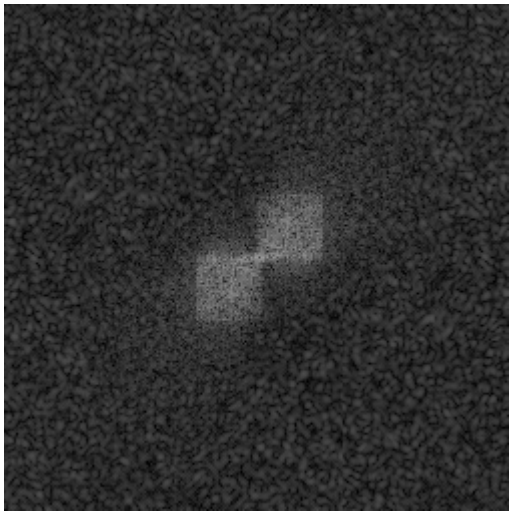

(d) FT of random pulse

Figure 3 – Occluded images and their Fourier Transforms

10. REFERENCES

1. P. Kube, A. Pentland "On the Imaging of Fractal Surfaces", *IEEE Transactions on Pattern Analysis and Machine Intelligence*, Vol PAMI-10(5) September, 1988

2. H.O. Peitgen (Ed) The Science of Fractal Images, Berlin: Springer-Verlag (1988)

3. J. Feders Fractals, Plenum Press, New York, NY (1988)

4. S.P. Kozaitis, H.G. Andrews, W.E. Foor "Optical Image Analysis Using Fractal Techniques", SPIE Conference on *Analog Photonics*, paper 1790-15, Boston, MA, September 1992

5. R.F. Voss, "Random fractal forgeries," in Fundamental Algorithms for Computer Graphics, R.A. Earnshaw, Ed. Berlin: Springer-Verlag, (1985)